Journal of
Materials Chemistry A

Materials for energy and sustainability

Accepted Manuscript

This article can be cited before page numbers have been issued, to do this please use: H. Lyu, C. J. Jafta, I. Popovs, H. Meyer, J. A. Hachtel, J. Huang, B. G. Sumpter, S. Dai and X. Sun, *J. Mater. Chem. A*, 2019, DOI: 10.1039/C9TA04869C.

ROYAL SOCIETY OF CHEMISTRY

rsc.li/materials-a

View Article Online
DOI: 10.1039/C9TA04869C

A Dicyanobenzoquinone based Cathode Material for Rechargeable Lithium and Sodium Ion Batteries

Hailong Lyu,[ad] Charl J. Jafta,[a] Ilja Popovs,[a] Harry M. Meyer III,[b] Jordan A. Hachtel,[c] Jingsong Huang,*[c] Bobby G. Sumpter,[c] Sheng Dai,[ad] Xiao-Guang Sun*[a]

[a] Chemical Sciences Division, Oak Ridge National Laboratory, Oak Ridge, Tennessee 37831, USA

[b] Materials Science and Technology Division, Oak Ridge National Laboratory, Oak Ridge, Tennessee 37831, USA

[c] Center for Nanophase Materials Sciences and Computational Sciences & Engineering Division, Oak Ridge National Laboratory, Oak Ridge, TN 37831, USA

[d] Department of Chemistry, University of Tennessee, Knoxville, TN 37996, USA

Corresponding Authors: huangj3@ornl.gov; sunx@ornl.gov

View Article Online
DOI: 10.1039/C9TA04869C

federally sponsored research in accordance with the DOE Public Access Plan (http://energy.gov/downloads/doe-public-access-plan).

ABSTRACT: Organic quinone materials offer a sustainable approach for electric energy storage, however, their intrinsic electrical insulation and dissolution into the electrolyte during cycling have hampered their wide application. To tackle these two issues, we have synthesized novel organic cathode materials by anchoring a quinone compound, 2,3-dicyano-p-benzoquinone (DCBQ) with a high redox potential of 3.37 V *vs.* Li/Li^+, onto carbon nanotubes (CNTs) (CNTs-DCBQ) through a facile ‘‘grafting to’’ method. The elaborate combination of excellent electron conductivity and large surface area of CNTs and stable and reversible redox reaction of DCBQ enables CNTs-DCBQ delivering high reversible capacities of 206.9 and 175.8 mA h g^{-1} at a current density of 10 mA g^{-1} and also remarkable capacities of 110.2 and 82.1 mA h g^{-1} at a higher current density of 200 mA g^{-1} with a capacity retention approaching 100 % after 1000 cycles for lithium and sodium ion batteries, respectively.

Keywords: Carbon nanotubes, dicyanobenzoquinone (DCBQ), organic cathode, lithium-ion batteries, sodium-ion batteries

View Article Online
DOI: 10.1039/C9TA04869C

1. Introduction

Currently, lithium ion batteries (LIBs) and sodium ion batteries (SIBs) mainly depend on inorganic cathode materials, which still need improvement in power density, sustainability, as well as safety.[1-3] As alternatives, organic electrode materials have been intensively investigated for both LIBs and SIBs due to their advantages of sustainability, flexibility of structure design and environmental friendliness. [4-16] Among various organic materials, benzoquinone (BQ) and its derivatives have emerged as one of the most promising materials owing to their multiple electron-redox reactions with high theoretical capacities and high redox potentials.[17, 18] Unfortunately, intrinsic electrical insulation and dissolution in the electrolytes are the two major drawbacks obstructing the wide applications of the quinone based materials.[8, 19, 20] So far, different strategies have been utilized to surmount those two drawbacks, [8, 9, 21-32] however, limited success has been achieved in enhancing electronic conductivity and suppressing the solubility of the quinone based cathode materials.[17, 33, 34]

Herein, we report a new strategy to surmount those two drawbacks by grafting quinone derivatives on the carbon nanotubes (CNTs) that have been extensively investigated for high-performance LIBs due to their advantages of high electronic conductivity, excellent mechanical and chemical stability, facile chemical functionalization, and large specific surface areas.[28, 35-39] Our selection of 2,3-dicyano-p-benzoquinone (DCBQ) is prompted by the knowledge that cyano-containing species such as tetracyanoethylene (TCNE) and tetracyanoquiondimethane (TCNQ) are commonly used as strong electron acceptors that can elevate the redox potentials.[40, 41] Indeed, calculations using the validated G3MP2B3 composite method predict that 2,3-dicyano-p-benzoquinone (DCBQ) has an electron affinity (EA) of 3.21 eV, which is even higher than that of 2.69 eV for tetrafluoro-*p*-benzoquinone (TFBQ) and 2.79 eV for tetrachloro-*p*-benzoquinone

View Article Online
DOI: 10.1039/C9TA04869C

(TCBQ), [42, 43] despite the substitution number of 2 *vs.* 4 (validations and results are summarized in **Table S1** with their structures shown in **Figure S1**).[44] The obtained new cathode materials demonstrate outstanding reversible capacity and rate performance, as well as long cycling stability in both LIBs and SIBs.

2. Experimental

2.1. Materials

2,3-Dicyanohydroquinone (DCHQ, 95%) was purchased from Oakwood Chemical. Iodobenzene diacetate (IBDA, 95%) was purchased from AK Scientific. 2-Aminoethanethiol (C_2H_7NS, >95.0%) was purchased from TCI. Multi-walled carbon nanotube (CNTs, carbon >95%), acetic acid (AcOH, ≥99%), nitric acid (HNO_3, 70%), thionyl chloride ($SOCl_2$, ≥99%), N,N-Dimethylformamide (DMF, anhydrous, 99.8%), tetrahydrofuran (THF, anhydrous, ≥99.9%), potassium carbonate (K_2CO_3, ≥99.0%), *p*-Benzoquinone (BQ, ≥98%), ferrocene (98%) and tetrabutylammonium hexafluorophosphate ($TBAPF_6$, ≥99.0%) were purchased from Sigma-Aldrich. Dichloromethane (CH_2Cl_2, 99.5 %), chloroform ($CHCl_3$, 99.8 %) and sulfuric acid (H_2SO_4, 95-98%) were purchased from BDH. Battery grade ethylene carbonate (EC), diethyl carbonate (DEC), dimethyl carbonate (DMC), propylene carbonate (PC), lithium hexafluorophosphate ($LiPF_6$) and sodium hexafluorophosphate ($NaPF_6$) were obtained from BASF. All the chemicals and solvents were used directly without further treatment.

2.2. Synthesis

2.2.1. Synthesis of 2,3-dicyano-p-benzoquinone (DCBQ)

The redox-active DCBQ was synthesized from DCHQ by a novel liquid-phase oxidation process. In a typical synthesis, DCHQ (5 g) was first dispersed homogeneously in CH_2Cl_2 (80 ml) with ultrasound for 30 mins, followed by addition of IBDA (22 g) and AcOH (2 ml) with stirring.

View Article Online
DOI: 10.1039/C9TA04869C

After refluxing at 40 ℃ for 12 hrs, a transparent dark orange solution was obtained. The solvent and AcOH were then removed thoroughly by rotary evaporation to obtain an orange residue. DCBQ was purified by mixing the above residue with $CHCl_3$ (30 ml) and heated to boiling. It was then cooled to room temperature and placed in a refrigerator at 5 °C for 12 hrs. The solid was washed with $CHCl_3$, filtered and dried at room temperature under vacuum to obtain 3 g golden DCBQ powder in ~ 60% yield. ^{1}H NMR (400 MHz, $CDCl_3$, δ): 7.10 (s, 2H, Ar H).

2.2.2. Oxidation of CNTs (CNTs-COOH)

CNTs were oxidized in strong and oxidative acid medium to form oxygen-containing functional groups. Thus, CNTs (1.0 g) was dispersed in an acid mixture of H_2SO_4/HNO_3 (3:1, vol) for 30 mins under sonication. The acid suspension of CNTs was stirred for 24 hrs at room temperature in a sealed flask. The product was filtered and washed thoroughly with DI-water until pH = 7. The oxidized CNTs were obtained by freeze-drying under vacuum and designated as CNTs-COOH.

2.2.3. Thiol-functionalization of CNTs (CNTs-SH)

The thiol-modified CNTs were obtained by a two-step procedure. First, CNTs was chlorinated by reacting CNTs-COOH (1 g) in a mixture of $SOCl_2$ (100 ml) and anhydrous DMF (1 ml) at 70 °C for 24 hrs under nitrogen protection. Then, $SOCl_2$ was removed by vacuum distillation to obtain the chlorinated CNTs. Hereafter, THF (25 ml) and K_2CO_3 (1.35 g) were mixed with the chlorinated CNTs under sonication for 45 mins, followed by addition of 2-aminoethanethiol (0.75 g). The suspension was heated to reflux at 65 ℃ for 24 hrs under nitrogen. After reaction, it was cooled to room temperature and the solid was filtered and washed with THF and methanol to remove the excess reactants. The CNTs-SH product was obtained by drying under vacuum at 80 °C.

2.2.4. Grafting of DCBQ onto CNTs (CNTs-DCBQ)

View Article Online
DOI: 10.1039/C9TA04869C

The DCBQ functionalized CNTs were prepared by the conjugate addition reaction of mercapto groups to DCBQ. [45] Briefly, CNTs-SH (1 g) was dispersed in a solution of methanol (50 ml) and DCBQ (1.58 g) for 30 mins under sonication. After refluxing at 65 ℃ for 12 hrs, IBDA (6.44 g) was added to oxidize the anchored DCBQ. The suspension was refluxed for another 12 hrs with stirring. The final product of CNTs-DCBQ was obtained by filtration, washing with methanol, and drying at 60 °C under vacuum. Similarly, the BQ functionalized CNTs (CNTs-BQ) were synthesized following the above procedure.

2.3. Characterization

^{1}H nuclear magnetic resonance (NMR) spectra was obtained on a Bruker Advance 400 MHz spectrometer using $CDCl_3$ as the solvent. The chemical structures of the fabricated products were characterized by Fourier transform infrared (FTIR) spectroscopy, whereas their thermal properties were evaluated by thermogravimetric analysis (TGA). TGA was carried out on a Perkin Elmer instrument from the ambient temperature to 800 °C in the nitrogen atmosphere at a heating rate of 10 °C min^{-1}. The morphologies and microstructures of the samples were observed by a Zeiss Merlin VP Scanning Electron Microscope (SEM) operating at 10 kV. The elemental compositions of the products were analyzed by energy dispersive X-ray spectroscopy (EDS) on a SEM instrument with an EDAX accessory. Nitrogen adsorption isotherms were measured at -196 ºC using TriStar 3000 volumetric adsorption analyzer manufactured by Micromeritics Instrument Corp. (Norcross, GA). Before adsorption measurements, the as-prepared samples were degassed in flowing nitrogen at 150 ºC for 12 h. The specific surface area of the samples was calculated using the Brunauer-Emmett-Teller (BET) method within the relative pressure range of 0.05 to 0.20. The X-ray photoelectron spectrometer (XPS) used for obtaining the XPS spectra is a Thermo Scientific (Waltham, MA, USA) Model K-Alpha instrument. This anode utilized is a

View Article Online
DOI: 10.1039/C9TA04869C

monochromated, micro-focusing Al Kα X-ray source (1486.6 eV). The XPS samples of cycled electrodes were prepared by dissembling the coin cells after cycling in an argon-filled glovebox. The obtained electrodes were washed several times with N-methylpyrrolidone (NMP) to dissolve the binder and obtain the powder samples for XPS measurements. The STEM measurement was carried out using the aberration-corrected (equipped with fifth-order aberration corrector) Nion UltraSTEM 100 (operated at 60 kV). The samples were deposited on a carbon support TEM grid by solvent casting.

2.4. Electrochemical measurements

The electrodes of modified CNTs were obtained by casting well homogenized slurries of active material and polyvinylidene fluoride (PVDF) binder with a weight ratio of 94:6 in N-methylpyrrolidone (NMP) on aluminum foils. After solvent evaporation, the electrodes were cut into discs with a diameter of 12 mm and dried thoroughly in a vacuum oven at 120 °C for 12 h. The as-prepared electrodes have similar active material loading of 1.6 mg/cm^2. The electrodes of DCBQ were papered following the same procedure with a mass ratio of DCBQ, C45, and PVDF of 6:3:1. All the coin cells for electrochemical measurement were assembled in an argon filled glove-box with the oxygen and moisture levels below 0.5 ppm. LIB half-cells were assembled with the modified CNTs electrodes as the cathode, lithium metal foils as both counter and reference electrodes, Celgard 2320 as separator and 1 M $LiPF_6$ dissolved in EC, DEC, and DMC (1:1:1, vol.) as the electrolyte. SIB half-cells were assembled with the modified CNTs electrodes as the cathode, sodium metal foil as both counter and reference electrodes, and Celgard 3401 as separator and 1 M $NaPF_6$ dissolved in PC as the electrolyte. The coin cells were galvanostatically cycled on a LAND CT2001A battery test system between 1.5 and 4.0 V at various current rates. Cyclic voltammogram (CV) data of the coin cells were recorded on a Biologic VSP instrument at a scan

View Article Online
DOI: 10.1039/C9TA04869C

rate of 0.5 mV s^{-1} in the voltage range of 1.5 - 4.0 V. CVs of BQ and DCBQ were obtained at a scan rate of 20 mV s^{-1} in the voltage range of -2.2 - 0.8 V vs. SCE by using two glassy carbon electrodes as the working and counter electrodes, a platinum wire as the reference electrode, and 0.05 M BQ or DCBQ in 0.5 M $TBAPF_6$ in DCM as the electrolyte. Ferrocene (0.48 V *vs.* SCE in DCM) was used to calibrate the relative potentials *vs.* SCE reference. Electrochemical impedance spectra (EIS) were measured on the same instrument with a voltage bias of 10 mV in the frequency range from 200 kHz to 10 mHz.

2.5. Theoretical calculations

Electron affinities (EAs) were calculated by using the G3MP2B3 composite method,[46] which was designed for the reliable predictions of thermochemistry. Using this method, B3LYP/6-31G* model chemistry was first used to optimize the geometries, and then to calculate the thermal energy corrections to Gibbs free energies. Afterwards, high level UQCISD(T)/BTBas1 theory was used to calculate the electron correlation corrections. Finally, the basis set extension corrections were calculated using UMP2/GTMP2Large method. Following these calculations, Gibbs free energies G° at 298.15 K and 1 atm were obtained for both neutral (q = 0) and anionic (q = -1) species of BQ, TFBQ, TClBQ, DCBQ, and DCBQ-SCH_3. EAs were obtained by taking the Gibbs energy difference between neutral and anionic species of each molecule. Infrared vibrational frequencies were calculated for various conformations of DCHQs and DCBQ using B3LYP/6-31G* model chemistry, following geometry optimizations. Frequencies reported were scaled using the recommended scaling factor of 0.96 for the corresponding model chemistry.[47] Frontier orbital energies were calculated for BQ, DCBQ, and DCBQ-SCH_3 using B3LYP, BHandHLYP and LC-wPBE functionals, along with 6-31G* basis set, all at the B3LYP/6-31G* optimized geometries. All calculations were done using the Gaussian 16 suite of programs.[48]

View Article Online
DOI: 10.1039/C9TA04869C

3. Results and Discussion

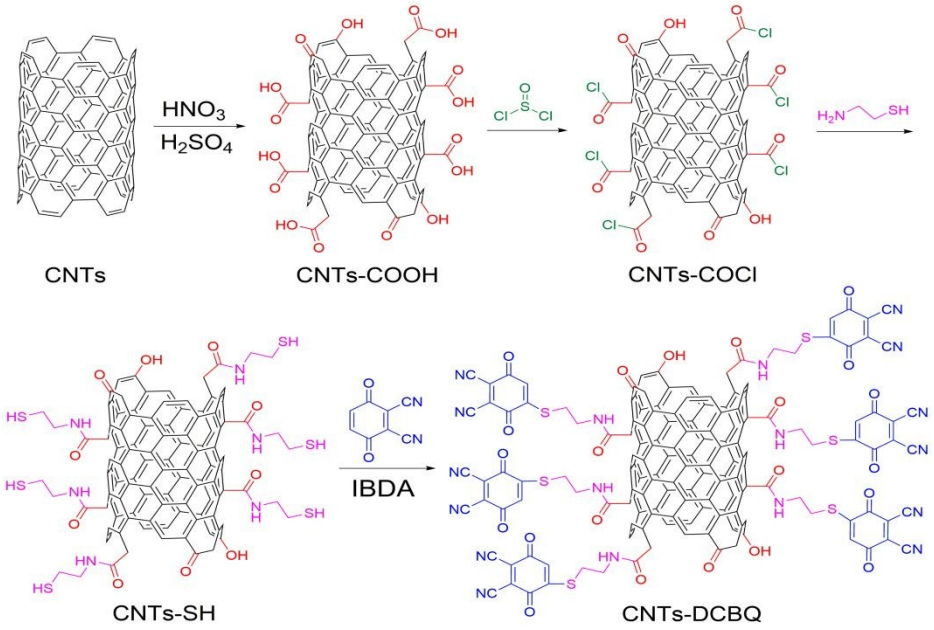

Scheme 1. Synthetic scheme for CNTs-DCBQ.

Small molecule DCBQ was synthesized by a facile liquid-phase oxidation of 2,3-dicyanohydroquinone (DCHQ) with iodobenzene diacetate (IBDA) (**Scheme S1**), instead of using highly toxic and insoluble heavy metal oxides such as MnO_2, Ag_2O, and Pb_3O_4 as the oxidant.[49-51] The structure of DCBQ was confirmed by FTIR spectra **(Figure S2a)** with all peaks assigned with the assistance of density functional theory (DFT) calculations (**Table S2** and **Figure S1**) and ^{1}H NMR spectra [(400 MHz, $CDCl_3$, δ): 7.10 (s, 2H, Ar H)].

DCBQ-functionalized CNTs (CNTs-DCBQ) were prepared for the first time using a ‘‘grafting to’’ approach with a thioether linkage as illustrated in **Scheme 1**.[45] The content of grafted DCBQ on the CNTs is estimated to be 14.62 wt%, based on the TGA plots of pristine CNTs, CNTs-COOH, CNTs-SH, CNTs-DCBQ and pure DCBQ (**Figure S3**). **Figure 1a** shows the scanning

View Article Online
DOI: 10.1039/C9TA04869C

electron microscopy (SEM) image of CNTs-DCBQ and the corresponding energy dispersive spectroscopy (EDS) elemental mapping. The nanotube morphologies in CNTs-DCBQ are almost identical to those in pristine CNTs and those in CNTs-COOH and CNTs-SH (**Figure S4**), indicating the structural integrity and dispersibility of the CNTs are barely affected by the multi-step modifications. This is also confirmed by the unaffected specific surface area of the functionalized CNTs, that is, 218.3, 226.8, 204.7, and 215.3 m^2 g^{-1} for CNTs, CNTs-COOH, CNTs-SH and CNTs-DCBQ, respectively **(Figure S5)**. In addition, the EDS mapping of CNTs-DCBQ shows uniform distribution of the key elements of C, N, O and S (**Figure 1a**). To further confirm the successful graft of DCBQ on CNTs, X-ray photoelectron spectra (XPS) of DCBQ, CNTs-SH and CNTs-DCBQ were also measured. As shown in **Figure 1**, both C1s and N1s spectra confirms the existence of C≡N in CNTs-DCBQ,[52, 53] while the S2p spectra confirms the linkage between CNTs and DCBQ.

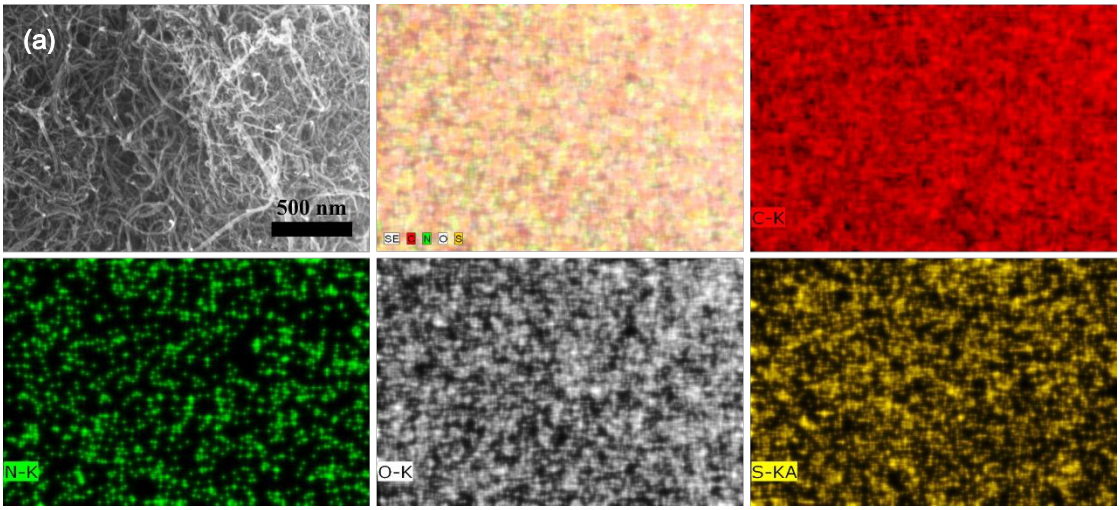

View Article Online
DOI: 10.1039/C9TA04869C

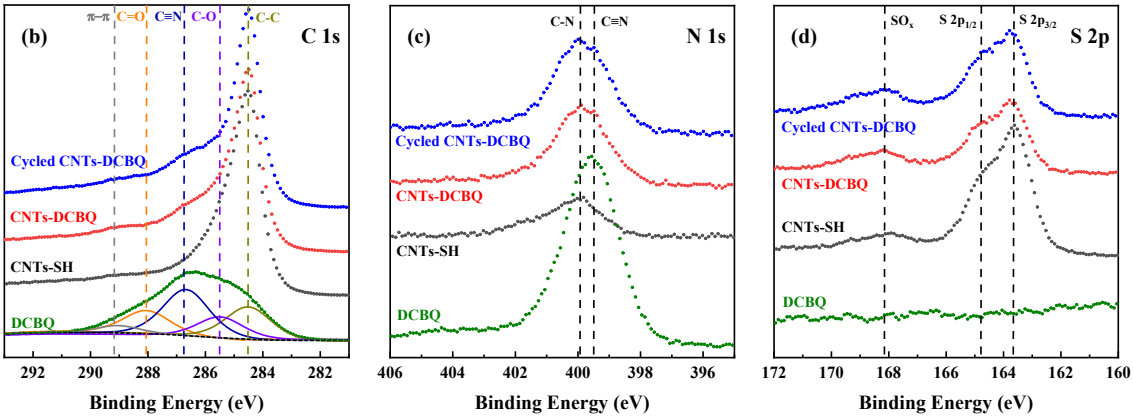

Figure 1. a) SEM image of CNTs-DCBQ (top left frame), as well as its total and individual EDS mapping of elements C, N, O and S; X-ray photoelectron spectra (XPS) of b) C1s, c) N1s and d) S2p for DCBQ, CNTs-SH, pristine and cycled CNTs-DCBQ.

Figure 2a shows the cyclic voltammograms (CVs) of the CNTs, CNTs-COOH, CNTs-SH and CNTs-DCBQ electrodes at a scan rate of 0.5 mV s^{-1} in the voltage range of 1.5-4.0 V *vs.* Li/Li^+. Nearly rectangular CV shapes are observed for CNTs and CNTs-COOH, indicating typical electrochemical capacitor behavior. Meanwhile, the CV of CNTs-COOH shows a much larger loop area than that of CNTs, due to the pseudo-capacitance through the Faradaic reactions of the surface oxygen-containing functional groups of CNTs-COOH. For CNTs-SH, in addition to the rectangular CV curve, a small oxidation peak at 2.65 V is observed, which may be attributed to the oxidation of the thiol groups to disulfide bonds. However, the absence of the corresponding reduction peak reveals poor reversibility of this redox reaction. For CNTs-DCBQ, two reduction peaks at 2.65 and 2.30 V and two corresponding oxidation peaks at 2.80 and 3.15 V are observed, though the latter two peaks are not well separated as the former ones. **Figure 2b** shows the typical charge–discharge profiles of the LIB half-cells at a current density of 10 mA g^{-1} based on the total

View Article Online
DOI: 10.1039/C9TA04869C

weight of the electrode. The overall slope profiles of all the curves are consistent with the electrochemical capacitor behavior of the CNTs based materials, whereas the plateaus of the CNTs-DCBQ material are consistent with the redox peaks shown in **Figure 2a and Figure S6**. It is noted that the specific capacity of CNTs-DCBQ is 170 mA h g^{-1} based on the total weight of the electrode loading, which is combination of the redox reactions of DCBQ, the Faradaic reactions of the surface oxygen functional groups, and the super capacitance adsorption on the surface of the CNTs.[35, 54] It is calculated that 28.2 % (47.9 mAh g^{-1}), 55.4 % (94.2 mAh g^{-1}) and 16.4 % (27.9 mAh g^{-1}) of the total capacity of CNTs-DCBQ is from the redox reactions of DCBQ, the Faradaic reactions of the surface oxygen functional groups and the super capacitance adsorption on the surface of the CNTs, respectively (see ESI for details). According to 14.62 wt.% of DCBQ in CNTs-DCBQ, the specific capacity from DCBQ is calculated to be 328 mAh g^{-1}, which is close to its theoretical capacity of 339 mAh g^{-1}.

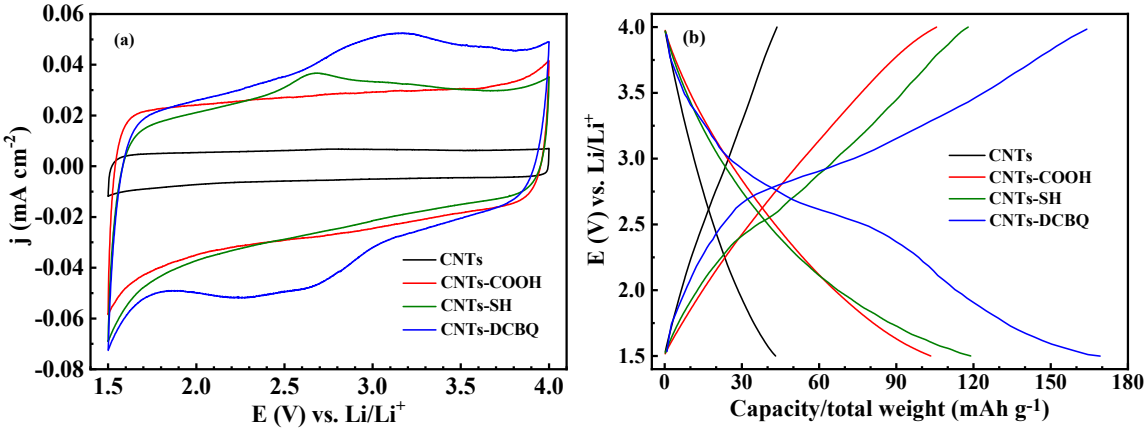

Figure 2. Cyclic voltammograms (CVs) of LIB half-cells of a) CNTs, CNTs-COOH, CNTs-SH and CNTs-DCBQ at a scan rate of 0.5 mV s^{-1}; Charge–discharge profiles of b) CNTs, CNTs-COOH, CNTs-SH and CNTs-DCBQ at a current density of 10 mA g^{-1}.

View Article Online
DOI: 10.1039/C9TA04869C

To better understand the electrochemical redox behavior of the CNTs-DCBQ, CVs of DCBQ and BQ monomers were also measured. As shown in **Figure S7,** two pairs of redox peaks are observed for DCBQ, centering at 0.08 and -0.83 V *vs.* SCE (equivalent to 3.37 and 2.46 V *vs.* Li/Li^+) with a peak separation of 0.21 V. In comparison, the redox peaks of BQ are located at lower potentials of -0.64 and -1.41 V *vs.* SCE (equivalent to 2.65 and 1.88 V *vs.* Li/Li^+) with a peak separation of 0.25 V. The average potential difference of 0.65 V between the redox peaks of BQ and DCBQ confirms the exceptional redox potential enhancing effect of the cyano groups. We further examined the frontier orbitals, especially the lowest unoccupied molecular orbitals (LUMOs) of BQ, DCBQ, and DCBQ-SCH_3. DCBQ-SCH_3 was adopted as a simplified model of CNT-DCBQ, as DCBQs were anchored on CNTs through thioether bonds. **Figure 3** shows the LUMOs for BQ, DCBQ, and DCBQ-SCH_3, all of which display similar features except at the substitution sites by the cyano and methylsulfanyl groups. It is noteworthy that there is no orbital node between the cyano group and the BQ ring (not to be confused with the node within the cyano group), indicating an in-phase and bonding relationship between the cyano group and the BQ ring. In contrast, when DCBQ is further substituted by a methylsulfanyl group, the corresponding LUMO displays an orbital node between the -SCH_3 group and the BQ ring, meaning an out-of-phase and antibonding relationship. The absence and presence of orbital nodes suggest that the LUMO orbital enegies should be decreased for DCBQ but increased for DCBQ-SCH_3, in line with the expected electron-withdrawing effect of the cyano groups and the electron-donating effect of the methylsulfanyl group. Indeed, DFT calculated LUMO energies by representative exchange-correlation functionals confirm the expected trend, showing that the LUMO of BQ is shallow, significantly deepened by the substitution of the cyano groups, and slightly increased by the further substitution of the methylsulfanyl group. By applying Koopmans' theorem,[55] the LUMO energies

View Article Online
DOI: 10.1039/C9TA04869C

correlate well with the electron affinities calculated by the validated G3MP2B3 composite method (**Figure S8**).

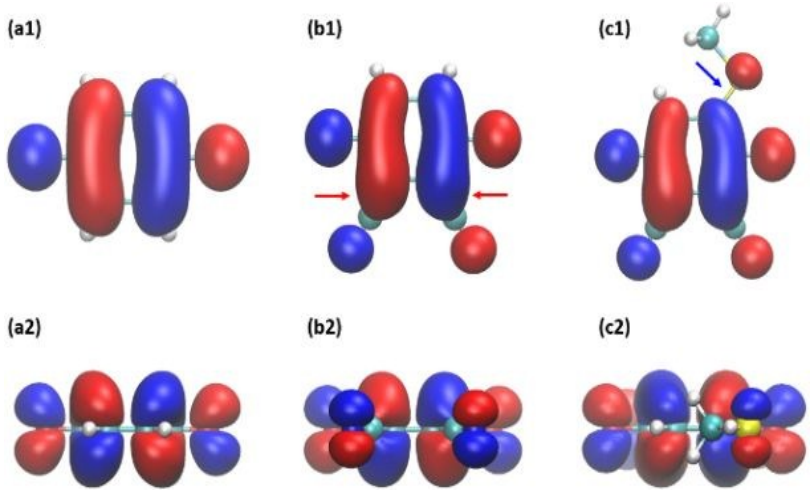

Figure 3. Top view (first row) and side view (second row) of the lowest unoccupied molecular orbital (LUMO) for a) BQ, b) DCBQ, and c) DCBQ-SCH_3 at an isosurface value of ±0.02 calculated with B3LYP/6-31G. The red and blue arrows indicate the absence and presence of orbital nodes.

Figure 4a shows the rate performance of the LIBs based on different functionalized CNTs. The initial capacity of the CNTs-DCBQ based LIB is over 200 mA h g^{-1} at a current density of 10 mA g^{-1}. After capacity fading in the first 10 cycles due to the formation of solid electrolyte (SEI) on the surface of the lithium anode and the cathode, the CNTs-DCBQ LIB exhibits reversible capacities of 151.3, 137.7, 125.0, 115.5, 102.8 and 87.3 mA h g^{-1} at current densities of 10, 20, 50, 100, 200 and 500 mA g^{-1}, respectively, with high coulombic efficiencies of 100% except in the rate changing cycles. In addition to good rate performance, the CNTs-DCBQ LIB exhibits superior cycling stability, as shown in **Figure 4b**. After a gradual capacity fading within the initial 50 cycles, the reversible capacity stabilizes at 110.2 mA h g^{-1} under a high current density of 200 mA g^{-1} and is still as high as 108.6 mA h g^{-1} after 1000 cycles, resulting in a capacity retention of 98.5 %. On

View Article Online
DOI: 10.1039/C9TA04869C

the other hand, the reversible capacities of the CNTs-COOH and CNTs-SH LIBs are 76.4 and 81.8 mA h g^{-1} after the initial stabilization cycles, and gradually decrease to 60.6 and 49.2 mA h g^{-1} after 1000 cycles, resulting in capacity retentions of 79.3% and 60.1%, respectively. The superior cycling performance of the CNTs-DCBQ LIB can be attributed to its unique structure that combines good electron conductivity of CNTs and excellent redox activity of the anchored DCBQ, preventing side reactions and dissolution into the liquid electrolyte during cycling. This is confirmed by the XPS spectra of the cycled CNTs-DCBQ sample, which is almost identical to that of the pristine CNTs-DCBQ (**Figure 2 & Figure S9**). As a comparison, the spectra of its close analog, the CNTs-BQ sample, change significantly before and after cycling, indicating severe structure damage taking place during cycling (**Figure S9**). [30] This result clearly indicates that the two cyano groups enhance the stability of CNTs-DCBQ.

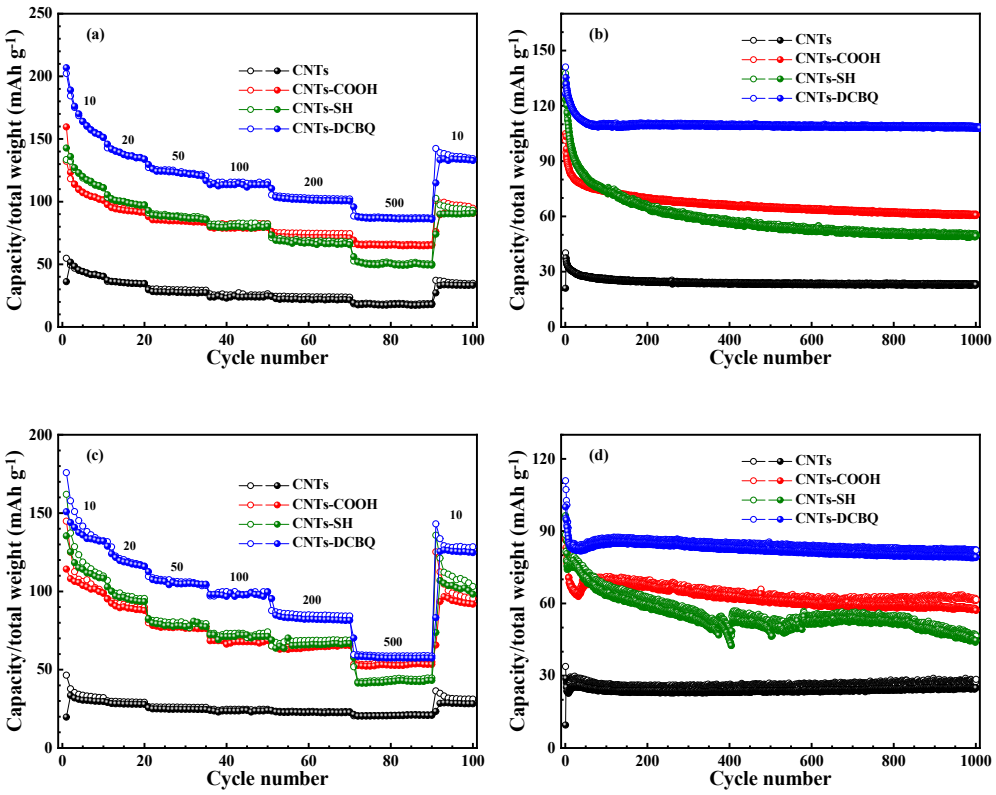

View Article Online
DOI: 10.1039/C9TA04869C

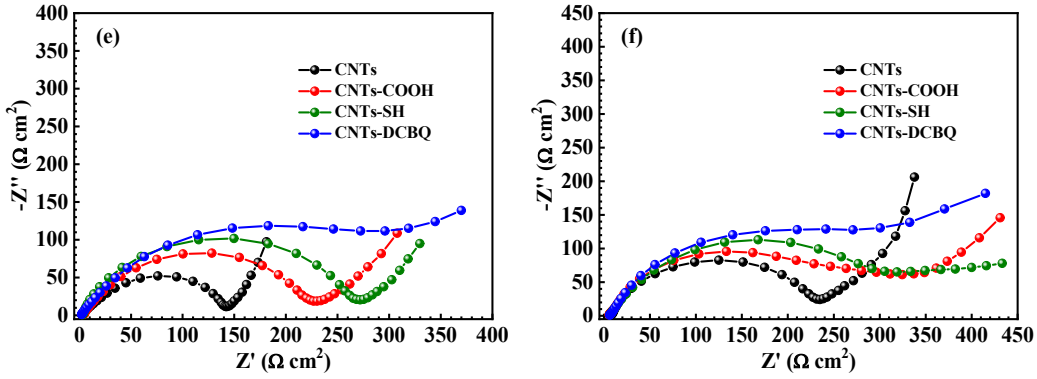

Figure 4. Charge–discharge capacities of the LIB (a, b) and SIB (c, d) half-cells based on CNTs, CNTs-COOH, CNTs-SH and CNTs-DCBQ at different current densities (mA g^{-1}) (a, c) and at a current density of 200 mA g^{-1} (b, d). (Hollow circles – and solid spheres □ represent charge and discharge capacities, respectively). Electrochemical impedance spectra (EIS) of the LIB half-cells based on CNTs, CNTs-COOH, CNTs-SH and CNTs-DCBQ (e) before cycling and (f) after 1000 cycles at 200 mA g^{-1}.

Figure 4c & 4d show the rate and cycling performance of the SIB half-cells, with their CVs shown in **Figure S10**. Generally, the SIBs exhibit similar trends as those of the LIBs (**Figure 4a & 4b)**, except that lower specific capacities are observed at the same current rates. For example, the initial capacity of the CNTs-DCBQ SIB is 175.8 mA h g^{-1} by the total weight of the electrode at a current density of 10 mA g^{-1}. The lower capacities of the SIBs than those of the LIBs under the same current rates can be attributed to the lower ionic conductivity of the electrolyte and slower reaction kinetics of the larger Na^+ ion (**Figure S11)**. Meanwhile, the CNTs-DCBQ SIB also exhibits a very stable cycling performance with an almost indiscernible capacity decay after 1000 cycles at 200 mA g^{-1} and retains nearly 100% of the 50th cycle's capacity. One noted common feature of the SIBs in **Figure 4d** is the gradual capacity increase after the initial capacity drop, which is absent for the LIBs in **Figure 4b**. This feature might be related to the high reactivity and soft nature of the sodium anode electrode.

View Article Online
DOI: 10.1039/C9TA04869C

The outstanding cycling stability of the CNTs-DCBQ cathode is also supported by the electrochemical impedance spectra (EIS) data shown in **Figure 4e & 4f**. The total cell impedances of the fresh LIBs increase with functionalization of the CNTs, that is, 142.2, 226.7, 268.1 and 272.3 Ω cm^2 for CNTs, CNTs-COOH, CNTs-SH and CNTs-DCBQ, respectively, suggesting adverse effects of the insulating functional groups to the highly conductive CNTs. After 1000 cycles, the corresponding cell impedances change to 234.8, 311.3, 318.8, and 270.9 Ω cm^2, respectively. The stable impedance of the CNTs-DCBQ LIB confirms its remarkable structural stability and redox reversibility, consistent with the stable cycling performance in **Figure 4b**. Comparatively, the total impedances of the SIBs are several times higher than those of the corresponding LIBs **(Figure S12)**, attributed to the lower ionic conductivity of the former electrolyte (**Figure S11).**

To figure out the origin of the capacity decrease of the first 50 cycles in **Figure 4**, both fresh half cells and symmetric cathode cells based on CNTs, CNTs-COOH and CNTs-DCBQ were assembled and evaluated by CVs at a scan rate of 2 mV s^{-1} in the voltage range of 1.5 – 4.0 V and 0 - 2 V for the half cells and the symmetric cathode cells, respectively. The EIS of the cells was monitored during cycling. As shown in **Figure S13,** the EIS of the symmetric cathode cells continually increases with cycling, whereas that of the half cells stabilizes after 50 cycles, and then it tends to decrease with cycling. The gradual increase of the EIS of the half cells correlates well with the gradual decrease of the capacity within the first 50 cycles. As there are no surface functional groups on the pristine CNTs, the EIS increase of the symmetric CNT cell can only be attributed to the side reactions on the surfaces of the CNTs, resulting in SEI formation and the accompanied reduction of surface area, of which the latter is well correlated with the reduction of the capacities (Figure S13g). Based on the above observations, the gradual capacity decrease

View Article Online
DOI: 10.1039/C9TA04869C

within the first 50 cycles in **Figure 4** can only be attributed to the SEI formations at both lithium anode and CNTs-DCBQ cathode.

As shown **Table S4 and Figure S14,** the electrochemical performance of CNTs-DCBQ is much better than those of the quinone/CNTs composite materials such as the quinone encapsulated SWCNTs cathodes, [56, 57] the emodin/SCNT hybrid, [58] P($4VC_{86}$-*stat*-LiSS14)/CNT buckypaper composite electrodes [59] and PBDTD@CNT cathodes.[60] However, it should be noted that the area capacity of CNTs-DCBQ is relatively low (0.11 mAh cm^{-2}, **Figure S15**), which can be improved by grafting more functional groups and by increasing the loading of the active materials.

4. Conclusion

In summary, cathode materials based on DCBQ grafted CNTs (CNTs-DCBQ) have been successfully synthesized *via* a multi-step functionalization approach for application in LIBs and SIBs. The CNTs-DCBQ cathode exhibits a remarkable high-rate cycling stability, achieving high capacities of 110.2 and 82.1 mAh g^{-1} at a high current density of 200 mA g^{-1} for LIB and SIB, respectively. The superior electrochemical properties of CNTs-DCBQ result from the elaborate synergy of the high electronic conductivity and large surface area of the CNTs and the stable redox reversibility of the grafted DCBQ, providing an avenue to bridge the performance gap between batteries and electrochemical capacitors. Therefore, CNTs-DCBQ is a promising cathode material for the next-generation LIBs and SIBs.

Acknowledgements

This work was supported by the ORNL laboratory-directed research and development (LDRD) program. This work was also supported by the U.S. Department of Energy, Office of Science,

View Article Online
DOI: 10.1039/C9TA04869C

Basic Energy Sciences, Materials Sciences and Engineering Division. The electron microscopy work was performed through a user project at ORNL's Center for Nanophase Materials Sciences, which is a US Department of Energy Office of Science User Facility. Calculations used the resources of the Compute and Data Environment for Science (CADES) at ORNL and of the National Energy Research Scientific Computing Center, which are supported by the Office of Science of the U.S. DOE under Contract Nos. DE-AC05-00OR22750 and DE-AC02-05CH11231, respectively.

References:

1. L.-X. Yuan, Z.-H. Wang, W.-X. Zhang, X.-L. Hu, J.-T. Chen, Y.-H. Huang and J. B. Goodenough, *Energy Environ. Sci.*, 2011, **4**, 269-284.
2. J. M. Tarascon and M. Armand, *Nature*, 2001, **414**, 359-367.
3. J. Y. Hwang, S. T. Myung and Y. K. Sun, *Chem. Soc. Rev.*, 2017, **46**, 3529-3614.
4. J. L. Wang, J. Yang, J. Y. Xie and N. X. Xu, *Adv. Mater.*, 2002, **14**, 963-+.
5. K. Nakahara, S. Iwasa, M. Satoh, Y. Morioka, J. Iriyama, M. Suguro and E. Hasegawa, *Chem. Phys. Lett.*, 2002, **359**, 351-354.
6. W. Guo, Y.-X. Yin, S. Xin, Y.-G. Guo and L.-J. Wan, *Energy Environ. Sci.*, 2012, **5**, 5221-5225.
7. S. R. Sivakkumar, P. C. Howlett, B. Winther-Jensen, M. Forsyth and D. R. MacFarlane, *Electrochim. Acta*, 2009, **54**, 6844-6849.
8. H. Chen, M. Armand, M. Courty, M. Jiang, C. P. Grey, F. Dolhem, J.-M. Tarascon and P. Poizot, *J. Am. Chem. Soc.*, 2009, **131**, 8984-8988.
9. Z. P. Song, Y. M. Qian, X. Z. Liu, T. Zhang, Y. B. Zhu, H. J. Yu, M. Otani and H. S. Zhou, *Energy Environ. Sci.*, 2014, **7**, 4077-4086.
10. H. Lyu, J. Liu, S. Mahurin, S. Dai, Z. Guo and X.-G. Sun, *J. Mater. Chem. A*, 2017, **5**, 24083-24090.
11. C. X. Peng, G. H. Ning, J. Su, G. M. Zhong, W. Tang, B. B. Tian, C. L. Su, D. Y. Yu, L. H. Zu, J. H. Yang, M. F. Ng, Y. S. Hu, Y. Yang, M. Armand and K. P. Loh, *Nat. Energy*, 2017, **2**.
12. J. Xie, Z. L. Wang, Z. C. J. Xu and Q. C. Zhang, *Adv. Energy Mater.*, 2018, **8**, 1703509.
13. H. Lyu, P. Li, J. Liu, S. Mahurin, J. Chen, D. K. Hensley, G. M. Veith, Z. Guo, S. Dai and X. G. Sun, *ChemSusChem*, 2018, **11**, 763-772.
14. K. Amin, L. J. Mao and Z. X. Wei, *Macromol. Rapid Commun.*, 2019, **40**.
15. X. L. Fan, F. Wang, X. X. Ji, R. X. Wang, T. Gao, S. Y. Hou, J. Chen, T. Deng, X. G. Li, L. Chen, C. Luo, L. N. Wang and C. S. Wang, *Angew. Chem. Int. Ed.*, 2018, **57**, 7146-7150.
16. W. Luo, M. Allen, V. Raju and X. L. Ji, *Adv. Energy Mater.*, 2014, **4**, 1400554.
17. Y. W. Wu, R. H. Zeng, J. M. Nan, D. Shu, Y. C. Qiu and S. L. Chou, *Adv. Energy Mater.*, 2017, **7**.
18. B. Häupler, A. Wild and U. S. Schubert, *Adv. Energy Mater.*, 2015, **5**, 1402034.
19. W. W. Huang, Z. Q. Zhu, L. J. Wang, S. W. Wang, H. Li, Z. L. Tao, J. F. Shi, L. H. Guan and J. Chen, *Angew. Chem. Int. Ed.*, 2013, **52**, 9162-9166.
20. W. Xu, A. Read, P. K. Koech, D. H. Hu, C. M. Wang, J. Xiao, A. B. Padmaperuma, G. L. Graff, J. Liu and J. G. Zhang, *J. Mater. Chem.*, 2012, **22**, 4032-4039.
21. J. Xiang, C. Chang, M. Li, S. Wu, L. Yuan and J. Sun, *Crystal Growth & Design*, 2008, **8**, 280-282.
22. B. Genorio, K. Pirnat, R. Cerc-Korosec, R. Dominko and M. Gaberscek, *Angew. Chem. Int. Ed.*, 2010, **49**, 7222-7224.
23. M. Lee, J. Hong, H. Kim, H. D. Lim, S. B. Cho, K. Kang and C. B. Park, *Adv. Mater.*, 2014, **26**, 2558-2565.
24. Z. Lei, W. Wei-kun, W. An-bang, Y. Zhong-bao, C. Shi and Y. Yu-sheng, *J. Electrochem. Soc.*, 2011, **158**, A991-A996.

View Article Online
DOI: 10.1039/C9TA04869C

25. A.-L. Barrès, J. Geng , G. Bonnard, S. Renault , S. Gottis , O. Mentré, C. Frayret, F. Dolhem and P. Poizot, *Chem. Eur. J.*, 2012, **18**, 8800-8812.
26. A. Shimizu, H. Kuramoto, Y. Tsujii, T. Nokami, Y. Inatomi, N. Hojo, H. Suzuki and J.-i. Yoshida, *J. Power Sources*, 2014, **260**, 211-217.
27. Z. Song, Y. Qian, M. L. Gordin, D. Tang, T. Xu, M. Otani, H. Zhan, H. Zhou and D. Wang, *Angew. Chem. Int. Ed.*, 2015, **127**, 14153-14157.
28. A. Jaffe, A. S. Valdes and H. I. Karunadasa, *Chem. Mater.*, 2015, **27**, 3568-3571.
29. K. Pirnat, R. Dominko, R. Cerc-Korosec, G. Mali, B. Genorio and M. Gaberscek, *J. Power Sources*, 2012, **199**, 308-314.
30. T. Yokoji, H. Matsubara and M. Satoh, *J. Mater. Chem. A*, 2014, **2**, 19347-19354.
31. Y. L. Liang, Y. Jing, S. Gheytani, K. Y. Lee, P. Liu, A. Facchetti and Y. Yao, *Nat. Mater.*, 2017, **16**, 841-+.
32. X. W. Chi, Y. L. Liang, F. Hao, Y. Zhang, J. Whiteley, H. Dong, P. Hu, S. Lee and Y. Yao, *Angew. Chem. Int. Ed.*, 2018, **57**, 2630-2634.
33. Y. Liang, Z. Tao and J. Chen, *Adv. Energy Mater.*, 2012, **2**, 742-769.
34. K. C. Kim, *Ind. Eng. Chem. Res.*, 2017, **56**, 12009-12023.
35. H. R. Byon, B. M. Gallant, S. W. Lee and Y. Shao-Horn, *Adv. Funct. Mater.*, 2013, **23**, 1037-1045.
36. W. Choi, S. Ohtani, K. Oyaizu, H. Nishide and K. E. Geckeler, *Adv. Mater.*, 2011, **23**, 4440-+.
37. B. Ernould, M. Devos, J. P. Bourgeois, J. Rolland, A. Vlad and J. F. Gohy, *J. Mater. Chem. A*, 2015, **3**, 8832-8839.
38. C. H. Li, M. Nakamura, S. Inayama, Y. Ishii, S. Kawasaki, A. Al-zubaidi, K. Sagisaka and Y. Hattori, *Acs Omega*, 2018, **3**, 15598-15605.
39. J. Q. Wang, K. Tee, Y. H. Lee, S. N. Riduan and Y. G. Zhang, *J. Mater. Chem. A*, 2018, **6**, 2752-2757.
40. V. G. Zakrzewski, O. Dolgounitcheva and J. V. Ortiz, *J. Chem. Phys.*, 1996, **105**, 5872-5877.
41. Y. Hanyu and I. Honma, *Sci. Rep.*, 2012, **2**, 453.
42. C. K. Mann and K. K. Barnes, *Electrochemical reactions in nonaqueous systems*, Marcel Dekker, Inc., New York, 1970.
43. K. Sasaki, T. Kashimura, M. Ohura, Y. Ohsaki and N. Ohta, *J. Electrochem. Soc.*, 1990, **137**, 2437-2443.
44. T. Heinis, S. Chowdhury, S. L. Scott and P. Kebarle, *J. Am. Chem. Soc.*, 1988, **110**, 400-407.
45. K. Mori, S. Hama, T. Okamoto, T. Kishi and H. Sayo, *Acta pharm. nordica*, 1991, **3**, 57-59.
46. L. A. Curtiss, K. Raghavachari, P. C. Redfern, V. Rassolov and J. A. Pople, *J. Chem. Phys.*, 1998, **109**, 7764-7776.
47. K. K. Irikura, R. D. Johnson and R. N. Kacker, *J. Phys. Chem. A*, 2005, **109**, 8430-8437.
48. M. Frisch, G. Trucks, H. Schlegel, G. Scuseria, M. Robb, J. Cheeseman, G. Scalmani, V. Barone, G. Petersson and H. Nakatsuji, *Gaussian 16, revision A. 03*, 2016.
49. G.-R. Cai, Z. Guan and Y.-H. He, *Syn. Commun.*, 2011, **41**, 3016-3025.
50. J. Bruce, S. Fitzjohn and R. Pardasani, *Chemischer Informationsdienst*, 1981, **12**.
51. A. R. POURALI and A. GOLI, *J. Chem. Sci.* , 2011, **123**, 63-67.
52. G. Galeotti, M. Ebrahimi, J. Lipton-Duffin, J. M. MacLeod, S. Rondeau-Gagne, J. F. Morin and F. Rosei, *Phys. Chem. Chem. Phys.*, 2017, **19**, 10602-10610.
53. T. Nakayama, K. Inamura, Y. Inoue, S. Ikeda and K. Kishi, *Surf. Sci.*, 1987, **179**, 47-58.
54. S. Y. Kim, J. Hong, R. Kavian, S. W. Lee, M. N. Hyder, Y. Shao-Horn and P. T. Hammond, *Energy Environ. Sci.*, 2013, **6**, 888-897.
55. T. Koopmans, *Physica*, 1934, **1**, 104-113.
56. Y. Ishii, K. Tashiro, K. Hosoe, A. Al-zubaidi and S. Kawasaki, *Phys. Chem. Chem. Phys.*, 2016, **18**, 10411-10418.
57. L. Canghao, I. Yosuke, I. Shunya and K. Shinji, *Nanotech.*, 2017, **28**, 355401.
58. P. Hu, H. Wang, Y. Yang, J. Yang, J. Lin and L. Guo, *Adv. Mater.*, 2016, **28**, 3486-3492.
59. N. Patil, A. Aqil, F. Ouhib, S. Admassie, O. Inganäs, C. Jérôme and C. Detrembleur, *Adv. Mater.*, 2017, **29**, 1703373.
60. Y. Jing, Y. Liang, S. Gheytani and Y. Yao, *Nano Energy*, 2017, **37**, 46-52.